First-principles study of site preferences for Fe in $Sm(CoFeCuZr)_z$ permanent magnets

Bingjie Liu,[1] Hui Wang,[1,*] Cheng Xu,[1] Xiaopeng Liu,[2] Qianfan Zhang,[2] Tianli Zhang,[1] Plamen Stamenov,[3]
John Michael David Coey,[3] and Chengbao Jiang[1,†]

[1]*Key Laboratory of Aerospace Materials and Performance (Ministry of Education), School of Materials Science and Engineering,
Beihang University, Beijing, 100191, People's Republic of China*
[2]*School of Materials Science and Engineering, Beihang University, Beijing, 100191, People's Republic of China*
[3]*School of Physics, Trinity College, Dublin 2, CT 06106, Ireland*

$Sm(CoFeCuZr)_z$ permanent magnets are of great technological interest due to their good magnetic performance and excellent thermal stability. The Fe content plays a key role for magnetic properties, determining the maximum energy product and the highest working temperature. Here we investigated the Fe site preferences in $Sm(CoFeCuZr)_z$ magnets with Fe content up to 26 wt. %, the solubility limit in sintered magnets by first-principles calculations. It is shown that Fe dissolves preferably in the rhombohedral Th_2Zn_{17}-type (2:17 R) phases, with a strong preference for the dumbbell ($6c$) sites. After $6c$ sites are fully occupied, Fe distributes in $18f$ sites as scattered as possible. The crystal structures of 2:17 R type $Sm_2(Co, Fe)_{17}$ lattice were presented with varying Fe content. The calculated structure and magnetic properties were analyzed comparing with experimental results of 2:17 R phases in multicomponent alloys. Also, the gradually increased substitution energy with continuous doping explained the difficulty in preparation of $Sm(CoFeCuZr)_z$ magnets with much Fe.

I. INTRODUCTION

For decades, $Sm(CoFeCuZr)_z$ permanent magnets have attracted significant attention because of their good magnetic performance, excellent thermal stability and strong corrosion resistance, and they have been used commercially in many fields like aerospace, defense, and communication technologies, especially in high temperature applications [1–3]. It is well established that the microstructure of $Sm(CoFeCuZr)_z$ magnets consists of a Fe-rich $Sm_2(Co, Fe)_{17}$ matrix phase with Th_2Zn_{17}-type rhombohedral structure (2:17 R phase), a Cu-rich $Sm(Co, Fe)_5$ cell boundary phase with $CaCu_5$-type hexagonal structure (1:5 H phase), and a Zr-rich lamellar phase with $ZrCo_3$-type rhombohedral structure (1:3 R phase) [4,5]. The Fe-rich 2:17 R phase is responsible for the high remanence, the Cu-rich 1:5 H phase generates strong pinning of domain walls during the demagnetization process, resulting in the high coercivity of magnets [6–8], while the Zr-rich 1:3 R phase provides a diffusion path for Cu to 1:5 H phase and Fe to 2:17 R phase [9].

It should be noted that Fe has a significant effect on the magnetic properties of $Sm(CoFeCuZr)_z$ magnets [10]. On one hand, it influences room-temperature magnetic performance significantly. In general, higher Fe content is necessary for improved room-temperature performance of $Sm(CoFeCuZr)_z$ magnets. Much effort has been made to achieve a higher maximum energy product $(BH)_{max}$ through introducing more Fe into $Sm(CoFeCuZr)_z$ magnets [11–13]. For example,

Horiuchi *et al.* developed a $Sm(Co_{0.57}Fe_{0.35}Cu_{0.06}Zr_{0.02})_{7.8}$ alloy magnet with an ultrahigh $(BH)_{max}$ of $266\,kJ/m^3$ [14]. However, too much Fe promotes the precipitation of a soft $Zr_6(Fe, Co)_{23}$ cubic phase and the deterioration of uniaxial magnetocrystalline anisotropy of $Sm(CoFeCuZr)_z$, resulting in unavoidable drop of coercivity and magnetization loop squareness. On the other hand, Fe has an important influence on high temperature magnetic properties. [10]. Lower Fe content leads to a lower temperature coefficient of coercivity and a higher operating temperature, accompanied by a trade-off reduction of remanence and maximum energy product. In order to obtain an excellent high-temperature magnet with the optimized maximum energy product, Fe content must be controlled accurately.

For understanding the influence of Fe on structure and magnetic properties, it is necessary to establish a clear picture of the site preference of Fe in $Sm(CoFeCuZr)_z$ magnets at different doping contents. Because of the strong neutron absorption of Sm [15,16], it is impractical to determine the Fe site preferences in SmCo systems by neutron scattering. So far there are several experimental investigations of transition metal atoms like Fe, Cu, Zr, etc., -doped $SmCo_5$ and Sm_2Co_{17} compounds [17–20], while they are mostly focused on structure and magnetic properties. By density functional theory (DFT) calculations, Larson *et al.* emphasized that the large magnetic anisotropy energy (MAE) in $SmCo_5$ comes mostly from Sm f-shell anisotropy, stemming from an interplay between the crystal field and the spin-orbit coupling [21]. The reduced MAE in Sm_2Co_{17} with $SmCo_5$ is caused by the partial substitution of Sm by Co_2 dumbbells [22]. In addition, it is reported that Cu substitution is more favorable in the 1:5 than the 2:17 phase by Sabirianov *et al.* [23]. Mössbauer spectroscopy has been used by Nagamine *et al.* to show that

*huiwang@buaa.edu.cn
†jiangcb@buaa.edu.cn

Fe has a site preference for the 6*c* sites [24]. However, the detailed site preferences with different Fe content have not been studied in detail.

In this work, we carried out a systematical first-principles simulation of site preferences for Fe in 2:17 type SmCo permanent magnets. Fe is found to dissolve preferably in the 2:17 *R* phase, with a strong preference for 6*c* sites. When the 6*c* sites are fully occupied, excess Fe disperses on 18*f* sites as far as possible. The clear structural pictures of Fe substitution in 2:17 *R* phase are presented. Moreover, the calculated results of substitution energy, structural, and magnetic properties of $Sm_2(Co, Fe)_{17}$ have been discussed with commercial multicomponent alloys.

II. THEORETICAL AND EXPERIMENTAL DETAILS

First-principles calculations are carried out using the Vienna *Ab initio* Simulation Package (VASP) software [25]. It is well known that the DFT method [26] with projector-augmented wave potentials has prolific use for structural calculations [27]. The generalized gradient approximation (GGA) of Perdew, Burke, and Ernzerhof was employed for the correlation and exchange potentials [25]. In order to make sure that the total energies are converged within 10^{-6} eV per unit cell, an energy cutoff of 400 eV and $5 \times 5 \times 3$ *k*-mesh grids are used. For the correction of the on-site repulsive interaction, the transition element *f* electron states atoms were treated by the local density approximation+*U* method introduced by Dudarev [28]. Two kinds of pseudopotential, "Sm" and "Sm_3" were employed for Sm_2Co_{17} calculations, respectively. Full structure relaxation is performed at each configuration until the forces become lower than 0.01 eV/A.

Alloy ingots with nominal composition of $Sm(Co_{bal}Fe_vCu_{0.06-0.08}Zr_{0.02-0.03})_{7.6-7.8}$ ($v = 0-0.36$) have been prepared by arc melting under Ar atmosphere, followed by conventional powder metallurgy processing. The ingots are crushed and ball milled into powders with an average size of about 5 μm. The powders are then aligned and pressed in a magnetic field of 2 T and then further compacted by cold isostatic pressing. The green bodies are sintered at 1200–1250 °C for 2 h in Ar atmosphere, followed by diffusion solution heat treatment at 1150–1220 °C for 4–6 h. Final isothermal aging treatment is performed at 800–820 °C for 24 h, followed by slow cooling to 400 °C at 0.4 °C/min, and the samples are kept again at 400 °C for 10 h before cooling down to room temperature.

The crystalline phases of all the $Sm(CoFeCuZr)_z$ alloys are identified at room temperature using a Rigaku diffractometer (Rigaku Corporation, Tokyo, Japan) with Cu K_α radiation ($\lambda = 1.5418$ Å). X-ray powder diffraction (XRD) data used for structure analysis are collected by a step scan mode with a step width of $2\theta = 0.02°$ and a sampling time of 1 s. All the XRD patterns are analyzed with General Structure Analysis System (GSAS) program by employing the Rietveld refinement technique.

The magnetic properties of aged magnets are measured with a Quantum Design physical property measurement system-vibrating sample magnetometer under a magnetic field up to 9 T at room temperature.

III. RESULTS AND DISCUSSION

The crystal structure of Sm_2Co_{17} is shown in Fig. 1. It can be derived from $SmCo_5$ by appropriately replacing one third of the Sm atoms by dumbbell Co-Co pairs [22]. In the close-packed structure of Sm_2Co_{17} and $SmCo_5$ compounds, the doping atom Fe is expected to substitute Co due to the similar atomic size and physical properties [23]. In $SmCo_5$, there are two inequivalent Co sites 2*c* and 3*g*, while four inequivalent Co sites 9*d*, 18*f*, 18*h*, and 6*c* are found in Sm_2Co_{17} lattice.

For Sm_2Co_{17}, we constructed the calculation using the GGA+*U* method with the Hubbard *U* correction ($U = 6.5$ eV) and the exchange parameter $J = 0.8$ eV. Two kinds of pseudopotential, "Sm" including *f* electrons as valence electrons and "Sm_3" treating *f* electrons as core electrons, were employed for calculation, respectively. The optimized lattice parameters were compared for analysis. For the former one, $a = b = 8.35146$ Å and $c = 12.14396$ Å, while for the latter, $a = b = 8.34753$ Å and $c = 12.14082$ Å were obtained. Notice that, the lattice parameters are very close, indicating that Sm *f* electrons do not influence the optimized structure so much. Additionally, for compounds of Fe-doped Sm_2Co_{17}, it was found to be really quite difficult to get converged calculation by using a pseudopotential of "Sm". In this scenario, it is reasonable to construct the structure configurations of Fe doped Sm-Co ternary system by DFT calculations using pseudopotential of "Sm_3".

In order to compare the site preferences of Fe in 1:5 *H* and 2:17 *R* phases, we have first carried out total energy calculations with one Co atom being replaced by Fe in the $SmCo_5$ and Sm_2Co_{17} lattices. We choose a unit-cell of 72 atoms for $SmCo_5$, corresponding to $2 \times 2 \times 3$ unit cells, 12 formula units, and a unit-cell of 57 atoms (with three formula units) for Sm_2Co_{17} [23]. The substitutions are described using the following equations:

$$12SmCo_5 + Fe = Sm_{12}Co_{59}Fe + Co, \tag{1}$$

$$3Sm_2Co_{17} + Fe = Sm_6Co_{50}Fe + Co. \tag{2}$$

FIG. 1. Crystal structure of Sm_2Co_{17}.

- Sm (6*c*)
- Co (9*d*)
- Co (18*f*)
- Co (18*h*)
- Co (6*c*)
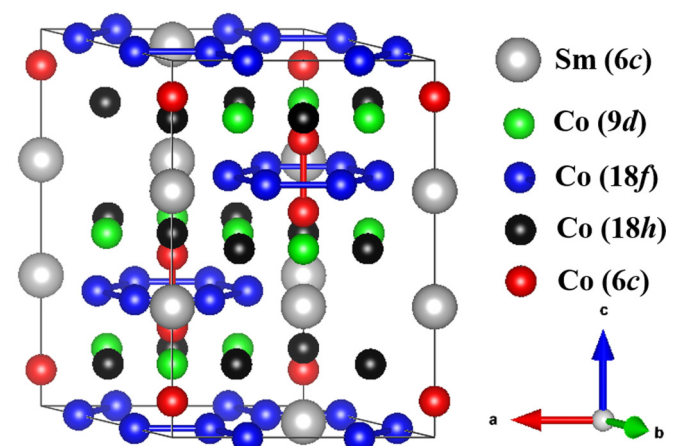
TABLE I. The calculated total energy, E_{sub} and the magnetic moments of $SmCo_5$ and Sm_2Co_{17} with one Fe substitution.

Compound	Energy (eV/supercell)	E_{sub} (eV)	Magnetic moments (μ_B/supercell)
$SmCo_5$	−486.93	0	84.01
Fe in $2c$ sites of $SmCo_5$	−488.25	0.17	85.22
Fe in $3g$ sites of $SmCo_5$	−488.21	0.21	84.96
Sm_2Co_{17}	−394.45	0	76.45
Fe in $6c$ sites of Sm_2Co_{17}	−395.81	0.13	77.34
Fe in $9d$ sites of Sm_2Co_{17}	−395.68	0.26	77.27
Fe in $18h$ sites of Sm_2Co_{17}	−395.69	0.26	77.41
Fe in $18f$ sites of Sm_2Co_{17}	−395.69	0.25	77.38

Then the energy of Fe substitution on Co sites is calculated based on

$$E_{sub} = E_{Sm_{12}Co_{59}Fe} - 12E_{SmCo_5} + E_{Co} - E_{Fe}, \quad (3)$$

$$E_{sub} = E_{Sm_6Co_{50}Fe} - 3E_{Sm_2Co_{17}} + E_{Co} - E_{Fe}. \quad (4)$$

In which the substitution energy, E_{sub} represents the total energy change of the system due to Fe substitution. The first and second items on the right side of the equations represent the total energy of the corresponding unit cells. And E_{Fe} and E_{Co} are the total energies per atom at 0 K for bulk Fe and Co, respectively. The total energies of pure elements Fe and Co are calculated in their standard states.

Table I shows the calculation results for one Co replaced by Fe in the $SmCo_5$ and Sm_2Co_{17} lattices, respectively. It is seen that the values of substitution energy for Fe in $SmCo_5$ and Sm_2Co_{17} are negative at all the crystal sites of Co. The lowest substitution energy occurs when Fe occupies $6c$ sites of Sm_2Co_{17}, suggesting that Fe prefers to dissolve in 2:17 R phase, which is in agreement with the experiment results [5].

As there are five elements, samarium, cobalt, iron, copper and zirconium in 2:17-type Sm-Co permanent magnets, then a question arises, as to which element holds the strongest preference for dumbbell sites? Table II shows the calculated energy with different elements occupying the dumbbell sites. Considering the larger atomic radius of samarium, one $6c$ Co_2 pair is replaced by one Sm atom. And according to previous reports [24], Zr occupies $6c$ sites in the form of Zr-vacancy pair. Notice that the calculations of the substitution energy of two Co atoms replacing the Co_2 pair in $6c$ sites is meaningless. The calculation results demonstrate that the energy of Fe substitution is the lowest among the five situations, indicating that Fe holds the strongest preference to occupy $6c$ sites in Sm(CoCuFeZr)$_z$ alloys. According to the Mössbauer

spectroscopy results [24], the dumbbell site in 2:17 R phase is the preferential site to be occupied by Fe atoms, which is consistent with our calculations.

Next, we carry out a systematic investigation on the site preference of Fe with increasing Fe content in the 2:17 R phase. It has to be mentioned that a basic principle we follow in the calculations is that different sites have different occupancy priorities: the doped atoms do not occupy other sites until the higher priority sites are fully occupied. Up to now, it is reported that in 2:17-type SmCo permanent magnets, Fe content can be up to about 26 wt. % [14], corresponding to $v = 0.35-0.36$ in $Sm(Co_{bal}Fe_vCu_{0.06}Zr_{0.02})_{7.6-7.8}$ magnets. This means that, in a 2:17 R unit cell, which holds three Sm_2Co_{17} molecules, i.e., $Sm_6Co_{51-n}Fe_n$, the maximum number n of doping Fe atoms is 18. Therefore, for the following investigation, we considered up to 18 Fe atoms occupying Co sites with n ranging from 1 to 18.

It has been known that Fe prefers to occupy $6c$ sites, suggesting that one to six atoms must distribute on dumbbell sites. There might be different arrangements of Fe atoms for values of $n \leqslant 6$. The structure exhibiting with the lowest energy determines the final distribution of Fe atoms.

For example, when doping two Fe there are two options for Fe distribution in $6c$ sites. One is to replace two Co atoms in the same dumbbell, forming one Fe-Fe dumbbell pair. The other is to replace two Co atoms belonging to different dumbbells, forming two Fe-Co dumbbells. The results of the calculations for the two cases are listed in Table SI ($n = 2$) [35]. It is seen that the case of two Fe-Co dumbbells is the more favorable. Similarly, for $n = 3$ there also are two possible crystal structures: one Fe-Fe dumbbell pair and one Fe-Co dumbbell pair, or three Fe-Co dumbbell pairs. The calculated results show that the latter is lower in energy, suggesting that the three Fe atoms tend to form three separate Fe-Co dumbbell pairs in the Sm_2Co_{17} lattice. For $n = 4$, the calculated results show that the fourth Fe prefers to occupy $6c$

TABLE II. The calculated energy, E_{sub} and the magnetic moments with different elements occupying Co-Co dumbbell sites in Sm(CoFeCuZr)$_z$ alloys.

Compound	Energy (eV/supercell)	E_{sub} (eV)	Magnetic moments (μ_B/supercell)
Sm in the $6c$ sites	−384.36	7.33	71.74
Co in $6c$ sites	−394.45	–	76.45
Cu in $6c$ sites	−390.73	2.49	74.62
Fe in $6c$ sites	−395.81	0.13	77.34
Zr in the $6c$ sites	−388.80	4.67	70.73
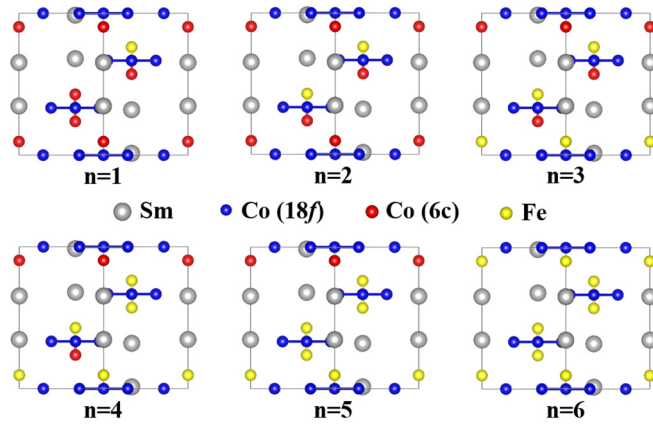
FIG. 2. Crystal structures of $Sm_6Co_{51-n}Fe_n$ ($n = 1-6$), which are viewed in the [110] direction. Yellow balls represent Fe atoms, blue ones represent Co ($18f$) atoms, red ones represent Co ($6c$) atoms, and light gray ones are Sm atoms. In order to show site preferences for Fe in $Sm_2(Co, Fe)_{17}$ lattice more clearly, the Co atoms on $9d$ and $18h$ sites are omitted in these pictures.

FIG. 3. Crystal structures of $Sm_6Co_{51-n}Fe_n$ ($n = 7-18$). Yellow balls represent Fe atoms, blue ones represent Co ($18f$) atoms, and light gray ones are Sm atoms. For clear display of site preference of Fe in $Sm_2(Co, Fe)_{17}$ lattice, the Co atoms on $9d$ and $18h$ sites are neglected in the structural pictures

sites than other sites like $9d$, $18f$, and $18h$ (Table SI, $n = 4$) [35], suggesting that Fe does not occupy other sites until the $6c$ sites are fully occupied.

We calculated all possible cases of Fe distribution in $6c$ sites, and listed calculation results in Supplemental Material Table SI [34,35]. The final crystal structures of $Sm_6Co_{51-n}Fe_n$ ($n = 1-6$) are shown in Fig. 2. In order to see the site preferences for Fe in the $Sm_2(Co, Fe)_{17}$ lattice more clearly, the Co atoms on $9d$ and $18h$ sites are omitted in our structural diagrams. It is found that Fe prefers to occupy $6c$ sites as far as possible. Until half the $6c$ sites are occupied by Fe, no Fe-Fe dumbbell pairs exist in $Sm_2(Co, Fe)_{17}$ lattice. This scattered distribution that generates the least structural and magnetic perturbation on the original Sm_2Co_{17} lattice, is the one with the lowest substitution energy.

How is Fe distributed after $n = 6$? Table III shows the calculation results for the seventh Fe in the other three Co sites ($9d$, $18f$ and $18h$). It is seen that the substitution energy is slightly lower than for the others when the seventh Fe occupies $18f$ sites, indicating its preference for the $18f$ sites.

As shown in Fig. 1, the $18f$ sites distribute on three equivalent hexagonal lattice planes. Different arrangements of Fe on these planes will generate different crystal structures. As with the study of Fe substitution in dumbbell sites, we carried out calculations of Fe distributions in $18f$ sites as a function of the number of doping atoms n, to obtain the structure configuration with the lowest substitution energy.

For example, there are four cases of Fe distribution, when doping eight Fe atoms. Six Fe atoms occupy the $6c$ sites, the

other two have four choices of arrangement on the $18f$ sites. Either two Fe atoms distribute in two $18f$ hexagonal planes, or two Fe atoms lie in the same hexagonal plane at different distances. The clear structural description and corresponding calculation results are listed in Table SII ($n = 8$) [35]. The lowest energy configuration is to place two Fe atoms across a diagonal in the same $18f$ lattice plane.

The optimized arrangements of $Sm_6Co_{51-n}Fe_n$ ($n = 7-18$) having the lowest energy are shown in Fig. 3. It is shown that Fe occupies $18f$ sites in the most scattered form: one, five, and six Fe atoms have only one occupation mode, while two are distributed across a diagonal, three are distributed on an equilateral triangle and four are distributed across two diagonals. In other words, Fe atoms are dispersed in each hexagonal lattice plane in the most scattered manner. The detailed calculation results for all possible site preference of Fe at $n = 7-18$ in the $Sm_2(Co, Fe)_{17}$ lattice are presented in Table SII [35]. The number of Fe atoms in the adjacent three hexagonal lattice planes with different n can be described as n (x, y, z), where x, y, z represents the number of farthest distributed Fe atoms in that three hexagonal planes accordingly. According to our calculations, the arrangement of n Fe atoms in $18f$ sites can be described as 7 (001), 8 (002), 9 (012), 10 (022), 11 (122), 12 (222), 13 (223), 14 (224), 15 (234), 16 (244), 17 (344), and 18 (444), correspondingly.

TABLE III. Calculation results of the different site preferences of the seventh Fe.

Compound	Energy (eV/supercell)	E_{sub} (eV)	Magnetic moments (μ_B/supercell)
The 7th Fe in $9d$ sites	−403.45	1.47	81.75
The 7th Fe in $18f$ sites	−403.50	1.41	81.91
The 7th Fe in $18h$ sites	−403.46	1.46	81.88
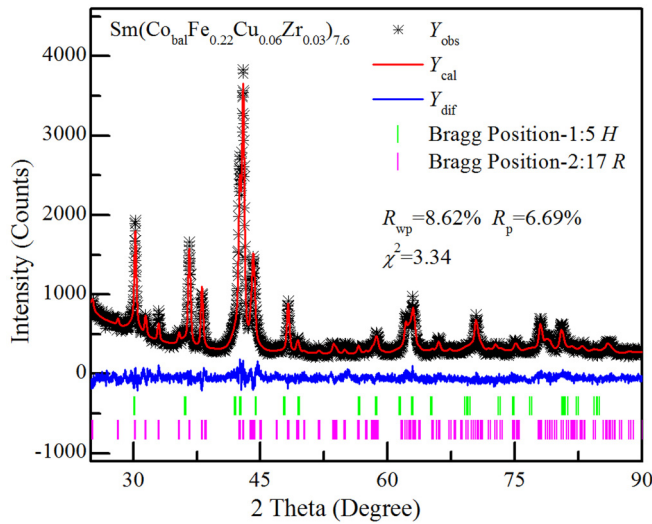
FIG. 4. Rietveld analysis for x-ray powder diffraction patterns of the milled $Sm(Co_{bal}Fe_{0.22}Cu_{0.06}Zr_{0.03})_{7.6}$ samples. Experimental data are shown as black fork dots, refined simulated patterns are shown as continuous red line. The difference between experimental data and fitted simulated pattern is shown as continuous blue line under each diffraction pattern. The Bragg positions are marked with vertical lines.

It can be speculated that the introduction of Fe changes the structural parameters, as well as the intrinsic magnetic properties of both ternary compounds $Sm_2(Co, Fe)_{17}$ and multicomponent $Sm(CoFeCuZr)_z$ alloys. In order to study the structural evolution of the 2:17 R phase in $Sm(CoFeCuZr)_z$ magnets and $Sm_2(Co, Fe)_{17}$ lattice, the lattice parameters a, c, c/a, and volume (V) are shown in Fig. 5. The lattice parameters of 2:17 R phase in $Sm(CoFeCuZr)_z$ magnets are obtained by Rietveld analyses of x-ray diffraction patterns, which are fitted to a mixture of $SmCo_5$ and Sm_2Co_{17}. Figure 4 shows an x-ray diffraction patterns along with Rietveld refined data. The small values of fitting parameters R_{wp}, R_p and χ^2 indicates the high reliability of the Rietveld analysis. All fitted x-ray diffraction patterns of $Sm(CoFeCuZr)_z$ samples are shown in Fig. S1 [35].

It is seen that doping of Fe enlarged the original lattice from Fig. 5. Note that the lattice parameter c of $Sm_2(Co, Fe)_{17}$ rarely increases for $n \leqslant 6$, but it increases for $7 \leqslant n \leqslant 18$. The reason for this may be that Fe prefers to occupy the $6c$ dumbbell sites, which control the c-axis parameter and the atomic radius of Fe is slightly small than Co. This is consistent with the calculated results for site preference.

As described before, we used two kinds of pseudopotential, "Sm_3" and "Sm" to calculate the magnetic moments and magnetic anisotropy energy (MAE) of Sm_2Co_{17}. It was shown that the total magnetic moments for the pseudopotential "Sm_3" (78.69 μ_B) is slightly smaller than the pseudopotential "Sm" (83.35 μ_B). The magnetic moments of Sm_2Co_{17} are shown in Table SIII [35]. The small difference between the two calculation results just lies in the spin moment of Sm f electrons. Nevertheless, both of them agree well with experimental result (83.4 μ_B) [29,30]. As for MAE calcula-
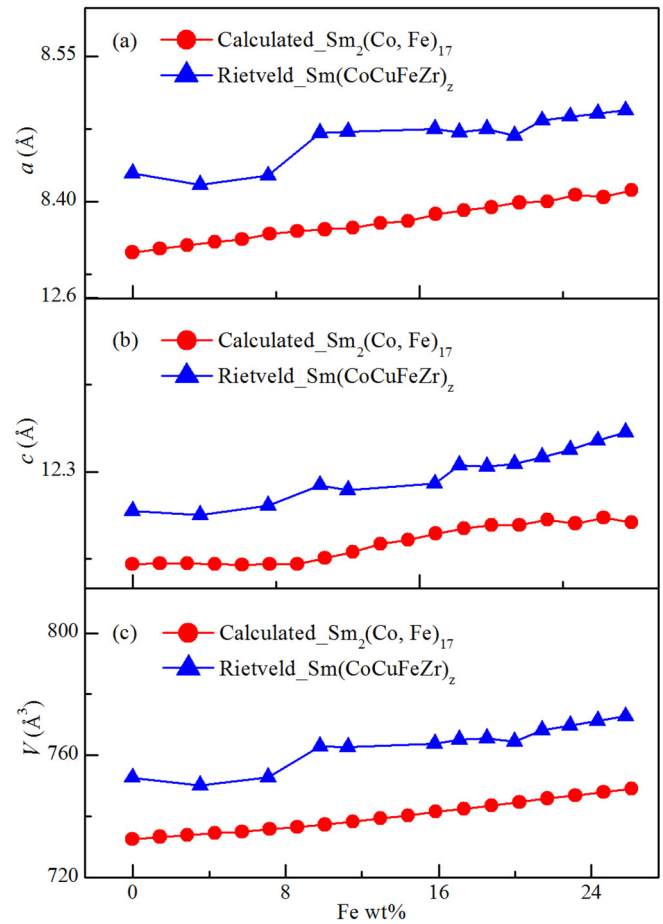
FIG. 5. Lattice constants of calculated results of $Sm_2(Co, Fe)_{17}$ and Rietveld results of 2:17 R phase in $Sm(CoFeCuZr)_z$ alloys.

tions, the MAE of 7.08 meV/f.u. is obtained by using the pseudopotential "Sm", which is very close to experimental result (6.42 meV/f.u.) [30]. As has been studied previously
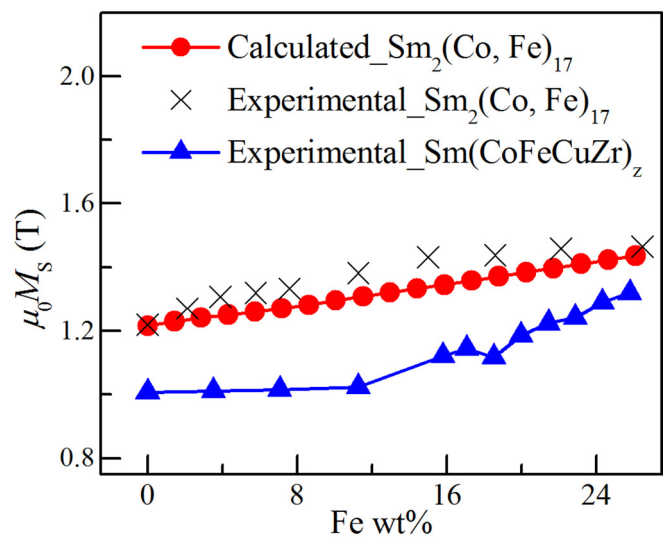
FIG. 6. Concentration dependence of the saturation magnetization $\mu_0 M_S$ of calculation and experimental [29,30] results for $Sm_2(Co, Fe)_{17}$, and experimental results for $Sm(CoFeCuZr)_z$ alloys.
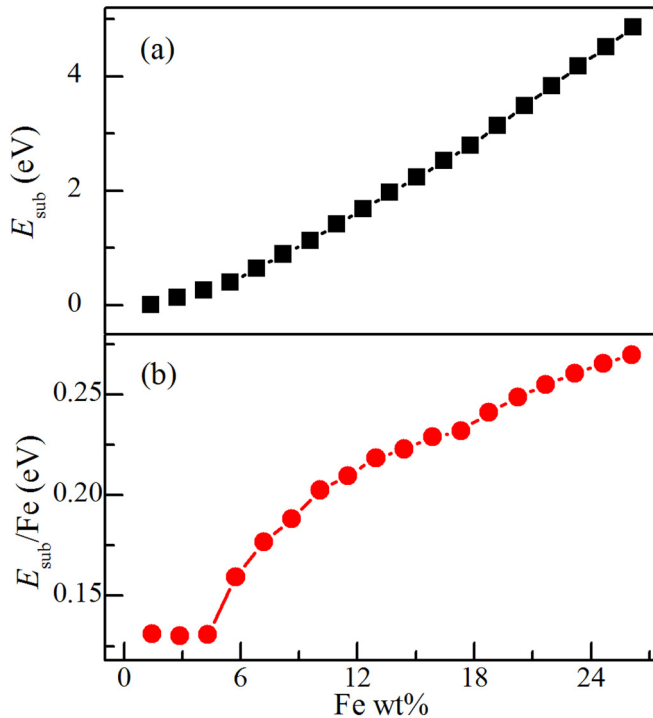
FIG. 7. Fe concentration dependence of the (a) substitution energy E_{sub} and (b) E_{sub} per Fe of $Sm_2(Co, Fe)_{17}$.

[21,22], the Sm f-shell anisotropy is found to play a very important role in the realization of magnetic anisotropy of Sm-Co magnets. It is not practical to get a proper result of MAE by pseudopotential "Sm_3" calculation.

Figure 6 shows the saturation magnetization $\mu_0 M_S$ of $Sm_2(Co, Fe)_{17}$ at different Fe content according to results in the literature [29,30], calculations, and experimental measurements of $Sm(CoFeCuZr)_z$ alloys. It is seen that the calculated saturation magnetization increases monotonically with increasing Fe content. The replacement of Co by Fe with larger magnetic moment does not destroy the ferromagnetic structure of the $Sm_2(Co, Fe)_{17}$ system. In addition, our calculated magnetization results are in good agreement with experiment, suggesting that the above site preference calculations are

valid and reliable. The difference between the experimental or calculated magnetization for $Sm_2(Co, Fe)_{17}$ and that of the sintered magnets is mainly due to the contribution of less-magnetic or nonmagnetic phases in the magnets.

Figure 7 shows the calculated change of the total substitution energy (a) and substitution energy change per Fe atom (b) as a function of Fe content. It is seen that the former increases with Fe content, suggesting that higher Fe substitutions become increasingly difficult, which is the reason why it is difficult to prepare $Sm(CoFeCuZr)_z$ magnets with more Fe [10,12,13,31]. There is a tendency to form other soft-magnetic Fe-rich phases [10,32–34] like Fe-Co or Fe-Co-Zr in multicomponent permanent magnets. It should be noted that the substitution energy per Fe is almost constant with $n < 3$. This explains why low-doped $Sm_2(Co, Fe)_{17}$ is usually easier to stabilize in the 2:17 R phase than undoped Sm_2Co_{17} [29].

IV. CONCLUSIONS

Detailed first-principles calculations of the Fe site preferences in 2:17-type SmCo permanent magnets establish that Fe is more soluble in the 2:17 R matrix phase than the 1:5 H cell boundary phase. Fe shows a strong preference for $6c$ sites, and only after they are fully occupied does it enter the $18f$ sites as a scattered manner. The lowest energy atomic configurations of $Sm_6Co_{51-n}Fe_n$ ($1 \leqslant n \leqslant 18$) are presented. The structural and magnetic properties of $Sm_2(Co, Fe)_{17}$ are compared with the 2:17 R phase in $Sm(CoFeCuZr)_z$ magnets. The high energy cost of replacing Co by Fe in Sm_2Co_{17} system helps to explain the difficulty in preparing $Sm(CoFeCuZr)_z$ magnets with high Fe content. In order to optimize $Sm(CoFeCuZr)_z$ magnets, with excellent magnetic properties at room temperature and good thermal stability, the iron content has to be controlled carefully.

[1] S. Liu, J. Yang, G. Doyle, G. Potts, and G. E. Kuhl, J. Appl. Phys. **87**, 6728 (2000).

[2] O. Gutfleisch, M. A. Willard, E. Bruck, C. H. Chen, S. G. Sankar, and J. P. Liu, Adv. Mater. **23**, 821 (2011).

[3] L. Liu, Z. Liu, M. Li, D. Lee, R. J. Chen, J. Liu, W. Li, and A. R. Yan, Appl. Phys. Lett. **106**, 052408 (2015).

[4] A. Yan, O. Gutfleisch, A. Handstein, T. Gemming, and K. H. Muller, J. Appl. Phys. **93**, 7975 (2003).

[5] X. Y. Xiong, T. Ohkubo, T. Koyama, K. Ohashi, Y. Tawara, and K. Hono, Acta Mater. **52**, 737 (2004).

[6] C. H. Chen, M. S. Walmer, M. H. Walmer, J. F. Liu, S. Liu, and G. E. Kuh, J. Appl. Phys. **87**, 6719 (2000).

[7] H. Sepehri-Amin, J. Thielsch, J. Fischbacher, T. Ohkubo, T. Schrefl, O. Gutfleisch, and K. Hono, Acta Mater. **126**, 1 (2017).

[8] R. Gopalan, K. Hono, A. Yan, and O. Gutfleisch, Scr. Mater. **60**, 764 (2009).

[9] M. Duerrschnabel, M. Yi, K. Uestuener, M. Liesegang, M. Katter, H. J. Kleebe, B. Xu, O. Gutfleisch, and L. Molina-Luna, Nat. Commun. **8**, 54 (2017).

[10] Z. H. Guo, W. Pan, and W. Li, J. Magn. Magn. Mater. **303**, e396 (2006).

[11] Y. Q. Wang, M. Yue, D. Wu, D. T. Zhang, W. Q. Liu, H. G. Zhang, and Y. H. Du, J. Alloy. Compd. **741**, 495 (2018).

[12] B. M. Ma, Y. L. Liang, J. Patel, D. Scott, and C.O. Bounds, IEEE Trans. Magn. **32**, 4377 (1996).

[13] S. Liu and A.E. Ray, IEEE Trans. Magn. **25**, 3785 (1989).

[14] Y. Horiuchi, M. Hagiwara, K. Okamoto, T. Kobayashi, M. Endo, T. Kobayashi, N. Sanada, and S. Sakurada, Mater Trans. **55**, 482 (2014).

[15] H. Kohlmann, T. C. Hansen, and V. Nassif, Inorg. Chem. **57**, 1702 (2018).

[16] J. Liu, P. Vora, P. Dent, M. Walmer, C. Chen, J. Talnagi, S. Wu, and M. Harmer, in *Proceedings of the Space Nuclear Conference* (Aerospace Nuclear Science and Technology (ANST), Boston, MA, USA, 2007).

[17] M. Merches, S. G. Sankar, and W. E. Wallace, J. Appl. Phys. **49**, 2055 (1978).

[18] M. V. Satyanarayana, H. Fujii, and W. E. Wallace, J. Appl. Phys. **53**, 2374 (1982).

[19] M. Q. Huang, W. E. Wallace, M. McHenry, Q. Chen, and B. M. Ma, J. Appl. Phys. **83**, 6718 (1998).

[20] A. Yan, A. Bollero, K. H. Muller, and O. Gutfleisch, Appl. Phys. Lett. **80**, 1243 (2002).

[21] P. Larson, I. I. Mazin, and D. A. Papaconstantopoulos, Phys. Rev. B **67**, 214405 (2003).

[22] P. Larson and I. I. Mazin, Phys. Rev. B. **69**, 012404 (2004).

[23] R. F. Sabirianov, A. Kasgyap, R. Skomski, S. S. Jaswal, and D. J. Sellmyer, Appl. Phys. Lett. **85**, 2286 (2004).

[24] L. C. C. M. Nagamine, H. R. Rechenberg, and A. E. Ray, J. Magn. Magn. Mater. **89**, L270 (1990).

[25] G. Kresse and J. Furthmüller, Phys. Rev. B **54**, 11169 (1996).

[26] P. Hohenberg and W. Kohn, Phys. Rev. **136**, B864 (1964).

[27] P. E. Blöchl, Phys. Rev. B **50**, 17953 (1994).

[28] S. L. Dudarev, G. A. Botton, S. Y. Savrasov, C. J. Humphreys, and A. P. Sutton, Phys. Rev. B **57**, 1505 (1998).

[29] H. F. Mildrum, M. S. Hartings, K. J. Strnat, and J. G. Tront, in *AIP Conference Proceedings*, No. 10 (AIP, New York, 1973), p. 618.

[30] R. Perkins, S. Gaiffi, and A. Menth, IEEE Trans. Magn. **11**, 1431 (1975).

[31] G. Xu, L. Peng, M. Zhang, J. Wang, Y. Fu, and L. Liu, Rare Metal. Mater. Eng. **37**, 396 (2008).

[32] G. C. Hadjipanayis, J. Appl. Phys. **55**, 2091 (1984).

[33] X. Y. Xiong and T. R. Finlayson, J. Iron Steel Res. Int. **13**, 154 (2006).

[34] K. Kumar, J. Appl. Phys. **63**, R13 (1988).

[35] See Supplemental Material at http://link.aps.org/supplemental/10.1103/PhysRevMaterials.4.044406 for detailed calculation results of Fe site preference, magnetic moments and Rietveld analysis for XRD patterns.